A Multi-State Dynamic Thermal Model for Accurate Photovoltaic Cell Temperature Estimation

Li, Chenxi; Spataru, Sergiu; Zhang, Kanjian; Yang, Yongheng; Wei, Haikun

Published in:
I E E E Journal of Photovoltaics

DOI (link to publication from Publisher):
10.1109/JPHOTOV.2020.2987401

Publication date:
2020

Document Version
Accepted author manuscript, peer reviewed version

A Multi-State Dynamic Thermal Model for Accurate Photovoltaic Cell Temperature Estimation

Chenxi Li, Sergiu Viorel Spataru, Kanjian Zhang, Yongheng Yang, *Senior Member, IEEE*, and Haikun Wei

***Abstract*—The photovoltaic (PV) cell temperature strongly affects the performance and efficiency of the entire PV module. Thus, the accurate estimation of the cell temperature plays an important role in the health monitoring and energy assessment of PV systems. This paper proposes a multi-state dynamic thermal model for PV modules, considering the heat-transfer mechanisms between the module and its environments, as well as between layers. The proposed model is benchmarked against field measurements at Aalborg University, Denmark. The results demonstrate the effectiveness of the model to characterize the internal behavior of the PV module under varying weather conditions. The performance of the proposed thermal model is also compared with prior-art models, i.e., two benchmark models, a one-state thermal model and two typical empirical equation-based models. The comparison further confirms that the estimation of cell temperature using the developed model is more accurate, presenting a reliable prediction of power production for further monitoring and diagnosis.**

***Index Terms*—PV module; Cell temperature; Multi-state estimation; Dynamic thermal model; Solar power generation.**

I. Introduction

RENEWABLE energy, including solar, wind and geothermal power, has received more and more attention owing to environmental concerns when using the conventional fossil fuel. The large amount of available solar energy makes it highly appealing. Photovoltaic (PV) modules, as one type of solar energy, absorb sunlight and generate direct current (DC) power. However, only a small proportion of the solar PV energy is converted into electricity, typically 5%-25%, and the remainder is either reflected or converted into heat [1], causing the temperature of the PV cells to increase.

In fact, the temperature has a significant impact on the PV module characteristics [2]. The temperature increase results in a larger short-circuit current and a smaller open-circuit voltage. The voltage decrease is more prominent than the current increase, leading to a lower overall output power [3], which corresponds to an efficiency decrease by approximately 0.22% for a temperature increase of 1°C [4]. It was reported in [5] that the fill factor, diode reverse saturation current, and diode ideality factor might also be affected by the temperature. In addition, the temperature is responsible for most of chemical reactions that degrade modules [6]. Hence, a reliable estimation of the module temperature is necessary to understand the degradation and in turn predict its lifetime.

Notably, the temperature under the Standard Test Condition (STC) is defined by the cell temperature T_c, rather than the ambient temperature T_a or other module temperatures, e.g., the backsheet temperature T_b. In practice, T_c is quite different from other temperatures and is difficult to measure in practice. According to [7], the temperature difference between T_a and T_c can be as high as 22 °C in outdoor tests. Therefore, with the direct substitution of the cell temperature by the ambient (as done in most literature), large errors may be introduced [8]. The difference further results in an over-predicted output power, which can lead to the false diagnosis of the PV modules. In general, an accurate determination of the cell temperature could assist the assessment of PV module performance and further help detect inherent faults.

The cell temperature is affected by various factors. Firstly, it is correlated with atmospheric parameters, e.g., T_a, irradiance level G, wind speed W_s, as illustrated in [9]. Secondly, according to [10], the cell temperature T_c is also affected by the module encapsulating material, which determines the glazing-cover transmittance τ and plate absorbance α. Moreover, it has been discussed in [11] that the particular installation conditions of the module is another factor. Additionally, the electrical operation point that the module is working in affects the cell temperature T_c as well [12]. These factors make the estimation of the cell temperature very challenging.

In the literature, attempts have thus been made to estimate the PV cell temperature. For example, in [7], T_c is roughly estimated from T_a and G by a linear relationship under steady-state conditions. While in practical applications, T_a and G always fluctuate dramatically. Another method to the cell temperature estimation is to use the Nominal Operation Cell Temperature (T_{NOCT}) [13], which is a common parameter to indicate the cell temperature. However, this model can give significant errors under loading and environmental conditions deviating from the Standard Reference Environment (SRE) [14]. In [10], a modified equation was adopted considering actual electrical loading and thermal losses, while the applicability of the equation is limited by the specific mounting

This work was supported by the National Key Research and Development Program of China (Grant No. 2018YFB1500802), the National Natural Science Foundation of China (Grant No. 61973083, No. 61773118 and No. 61703100), and the Fundamental Research Funds for the Central Universities. *(Corresponding author: Kanjian Zhang.)*

C. Li, K. Zhang, and H. Wei are with the Key Laboratory of Measurement and Control of CSE, Ministry of Education, School of Automation, Southeast University, Nanjing 210096, P.R. China (e-mail: chenxi_li@seu.edu.cn; kjzhang@seu.edu.cn; hkwei@seu.edu.cn).

S. V. Spataru and Y. Yang are with the Department of Energy Technology, Aalborg University, Aalborg 9220, Denmark (e-mail: ssp@et.aau.dk; yoy@et.aau.dk).

conditions [15]. A method was then presented in [16] by measuring the open-circuit voltage of the module, which is yet difficult to apply in practice. Another way is to use temperature sensors attached on the backsheet of modules, while T_c is higher than T_b. The difference depends on the module substrate materials and solar irradiance level. A simple expression to compensate for the difference was given in [17]. However, compared to the fluctuated T_b, T_c is less sensitive since the solar cells are enclosed within the module structure [18]. There were many explicit and implicit empirical correlations, as listed in [10], which express T_c as a function of the pertinent environment variables. It should be noted that the correlated parameters are usually system-dependent, which requires the users to select a suitable correlation with adjusted parameters.

In all, most of the above estimation methods are based on steady-state models, which assume that the PV module temperature follows the atmosphere conditions immediately. However, the temperature variation is very dynamic under rapidly changing conditions. The PV module gets heated up and cooled down gradually due to the large time constant [19]. This means that a steady-state model cannot be justified anymore, and a detailed thermal analysis of the PV module is necessary to predict the cell temperature variation [20]. Subsequently, an original thermal model for PV systems was introduced in [21] to estimate the module temperature, considering the main energy exchange processes. A similar thermal model was verified using experimental data both in winter and summer operation conditions [22]. A 3-dimensional (3D) numerical model was presented and validated in [23] to predict the thermal and electrical behavior of PV modules under given environmental and operational conditions.

However, in those dynamic models, it is assumed that the temperature is uniform throughout different layers in the module, since they characterize a global energy balance on the module with one equivalent thermal capacity. In other words, the cell temperature is supposed to be equivalent to the backsheet temperature, as well as the front glass temperature. To address this, the temperature response of the PV module was modeled as a resistive-capacitive (RC) circuit in [19] using the thermal resistance and capacitance to define the conductive heat transfer between layers. Furthermore, a comprehensive thermo-electric model was introduced in [24], where five sections are considered to represent the layer features. A numerical model was developed and validated in [25] considering the heat balance equations and different thermal and electrical parameters. Nevertheless, these thermal models barely incorporate measuring feedback for estimation.

In light of the above, a detailed multi-state model (MSM) accounting for the PV module dynamics is developed in this paper. The proposed model can accurately estimate the PV module operating temperature, where the measured backsheet temperature and environmental monitoring data are used. The equations are established according to a comprehensive thermo-electrical dynamic model of the PV module with different layers, which takes both module characteristics and heat exchange under variable environment parameters into account. The present state is updated from the previous state according to the dynamic equations with all monitored data to reflect the inertia effect. On the other hand, the proposed approach allows automated state correction with the difference between the measurement and the estimation. The estimated cell temperature is compared with the actual measurements under various weather conditions. To highlight the effectiveness of the proposed model, the estimated results are also benchmarked with prior-art models, i.e., the Sandia temperature model, NOCT model, a common one-state thermal model and two recent-developed empirical equation-based models.

The rest of the paper is organized as follows: In Section 2, the proposed dynamic model for PV modules is presented in detail. The developed model has three states, representing the temperatures of different physical layers of PV modules. The models used to complete the contrast experiment together with the adopted performance indices are given in Section 3. In Section 4, the experimental set-up is described, followed by a comparison of the estimated results with the measurements in Section 5, where simulation results of the output power with various models are also presented. Finally, concluding remarks are provided in Section 6.

II. Proposed Multi-state Dynamic Model

The PV module under study in this paper is REC 245 PE, which is a multi-crystalline module. The entire ensemble of this module is consisted of five layers: glass covering, ethylene vinyl acetate (EVA), silicon cells, EVA and polyester backsheet. These layers are embedded in an anodized aluminum frame, whose temperature effect is not modeled in the paper, as the low surface area with respect to the module area has a negligible effect on the temperature response. Due to the strong heat-transfer capacity of the EVA, which results in an ignorable temperature change when compared to other layers, three dominating layers are considered, i.e., the glass cover, the solar PV cells, and the backsheet layer.

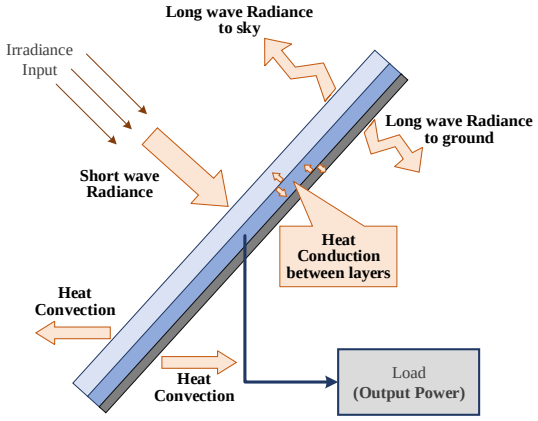

Fig. 1. Essential heat transfer processes of PV modules.

The conduction, convection and radiation heat exchanges between the PV module and its environments, as well as the load consumption are described in Fig. 1. In this paper, it is assumed that the temperature for each layer is uniformly distributed [1, 25] and the PV module operates under normal conditions (e.g., not considering the partial shading condition

or others). In this way, an average temperature is sufficient to express the overall operational state of the module. In fact, the mismatch between the outputs based on the monitored cell temperature and the measurements can be used to detect abnormal conditions. Based on the temperature model in [21], the heat balance for different layers can be described as:

For the glass cover:

$$A_m \cdot \rho_g \cdot d_g \cdot C_g \cdot \frac{dT_g}{dt} = A_m[\alpha_g \cdot G - h_{r,sky-g} \cdot (T_g - T_{sky}) - h_{cv,a-g} \cdot (T_g - T_a) - h_{cd,g-c} \cdot (T_g - T_c)] \quad (1)$$

in which A_m is the area of the module, ρ represents the density, d denotes the thickness, C is the heat capacity, the subscribe g indicates the properties of the front glass layer, $h_{r,sky-g}$ is the heat radiation coefficient between the glass and the sky that can be expressed by a nonlinear mapping relationship, and $h_{cd,g-c}$ is the heat conductive coefficient between the glass layer and the cell layer, which can be expressed by the inverse of $d_g/k_g + d_c/k_c$. Furthermore, the sky temperature T_{sky} is usually described in different forms of the ambient temperature under various weather conditions [24]. In (1), $h_{cv,a-g}$ is the heat convection coefficient between the glass and ambient, which is a function of the wind speed, and the most-common expression of $h_{cv,a-g} = 5.7 + 3.8 \times W_s$ is chosen in this paper.

To further simplify the analysis and modeling, a relatively straightforward and simple way has been adopted to evaluate the thermal radiation flux between the glass and sky as a ratio (α_1) of the thermal convection flux to obtain an analytical solution of the temperature [26]. In this way, (1) is modified as

$$A_m \cdot \rho_g \cdot d_g \cdot C_g \cdot \frac{dT_g}{dt} = A_m \cdot [\alpha_g \cdot G - (1+\alpha_1) \cdot h_{cv,a-g} \cdot (T_g - T_a) - h_{cd,g-c} \cdot (T_g - T_c)] \quad (2)$$

where the heat flux ratio α_1 is approximately equal to 0.2.

For the solar cells:

$$A_m \cdot \rho_c \cdot d_c \cdot C_c \cdot \frac{dT_c}{dt} = A_m \cdot [\tau_g \cdot \alpha_c \cdot G \cdot \beta - \left(h_{cd,c-g} \cdot (T_c - T_g) + h_{cd,c-b} \cdot (T_c - T_b)\right)] - P_m \quad (3)$$

in which the subscribe c indicates the properties of the PV cell layer, β is the fill factor, $h_{cd,c-b}$ is the heat conductive coefficient between the cell layer and backsheet that can be expressed by the inverse of $d_c/k_c + d_b/k_b$, and the output power P_m is simulated with the nominal power under STC considering the actual measurements of the irradiance and temperature. The reason for choosing this simple empirical model is that the PV module is supposed to work at the maximum power point under normal operating conditions.

For the backsheet:

$$A_m \cdot \rho_b \cdot d_b \cdot C_b \cdot \frac{dT_b}{dt} = A_m \cdot [\tau_g \cdot \alpha_b \cdot G \cdot (1-\beta) - h_{r,b-gnd} \cdot (T_b - T_{gnd}) - h_{cv,b-a} \cdot (T_b - T_a) - h_{cd,c-b} \cdot (T_b - T_c)] \quad (4)$$

where the subscribe b represents the properties of the backsheet layer, $h_{r,b-gnd}$ is the heat radiation coefficient between the backsheet and the ground, T_{gnd} indicates the temperature of the ground, and $h_{cv,b-a}$ denotes the heat convection coefficient between the backsheet and ambient. Considering that the thermal radiation flux between the backsheet and ground is a ratio (denoted by α_2) of the thermal convection flux, (4) can be modified as

$$A_m \cdot \rho_b \cdot d_b \cdot C_b \cdot \frac{dT_b}{dt} = A_m \cdot [\tau_g \cdot \alpha_b \cdot G \cdot (1-\beta) - (1+\alpha_2) \cdot h_{cv,b-a} \cdot (T_b - T_a) - h_{cd,c-b} \cdot (T_b - T_c)] \quad (5)$$

Taking the actual mounting situation, open-racked and low frame into account, the ratio α_2 is chosen as 0.52.

According to the datasheet, the thickness of the front glass is 3 mm with an area of 1.65 m^2. Certain material parameters of the layers are listed in Table 1 summarizing the preferences in [1, 24, 27, 28]. These parameters are assumed to be independent of the temperature.

TABLE 1
PARAMETERS USED TO ESTABLISH THE COMPREHENSIVE THERMAL MODEL

	Value		
	Front glass	Multi-crystalline solar cell	Polyester backsheet
d (m)	0.003	0.0003	0.0001
ρ (kg/m^3)	3000	2330	1200
C (J/kg·K)	500	677	1250
k (W/m·K)	1.8	148	0.2

To solve the above equations, including instantaneous irradiance level and ambient temperature, as well as wind speed, a dynamic model is established. The temperatures of different layers at the time instant k+1 are calculated as

$$T_i(k+1) = T_i(k) + sampling\ interval \cdot \frac{dT_i}{dt} \quad (6)$$

where k is the present-instant, and dT_i/dt is the temperature changes of different layers that can be calculated according to (2), (3), and (5).

When considering the state vector $\mathbf{x}(k)$ to represent the temperatures of different layers $[T_g\ T_c\ T_b]^T$ in Step k and the input vector $\mathbf{u}(k)$ to include the irradiance and ambient temperature, the dynamics of the PV module can be described by a multi-state model (MSM) that is expressed as

$$\begin{cases} \mathbf{x}(k+1) = f[\mathbf{x}(k), \mathbf{u}(k), \boldsymbol{\theta}(k)] + w(k) \\ y(k) = g[\mathbf{x}(k), \mathbf{u}(k), \boldsymbol{\theta}(k)] + v(k) \end{cases} \quad (7)$$

in which $\boldsymbol{\theta}(k)$ is consisted of constant materials parameters and the time-varying wind speed, $w(k)$ and $v(k)$ represent the noise terms related to sensor uncertainties subject to the Gaussian distribution, and $y(k)$ is an output (i.e., the measured backsheet temperature).

The next-instant state $\mathbf{x}(k+1)$ is then predicted based on the present state $\mathbf{x}(k)$ and the instantaneous input $\mathbf{u}(k)$ considering $\boldsymbol{\theta}(k)$. Actually, the measured backsheet temperature can be used as a feedback to correct the estimated state. In this way, the proposed MSM is improved by introducing an observer (i.e., MSM-O). Flowchart of the implementation procedure of the MSM-O is shown in Fig. 2.

III. BENCHMARK MODELS AND PERFORMANCE INDICES

Numerous models to estimate the PV module temperature have been proposed in the literature. In this section, to highlight

the effectiveness of the proposed model, it is compared with five representative ones, which are briefly described in the following. The two benchmark models are the Sandia thermal model and NOCT model. Those are the most commonly and widely used for module temperature correction.

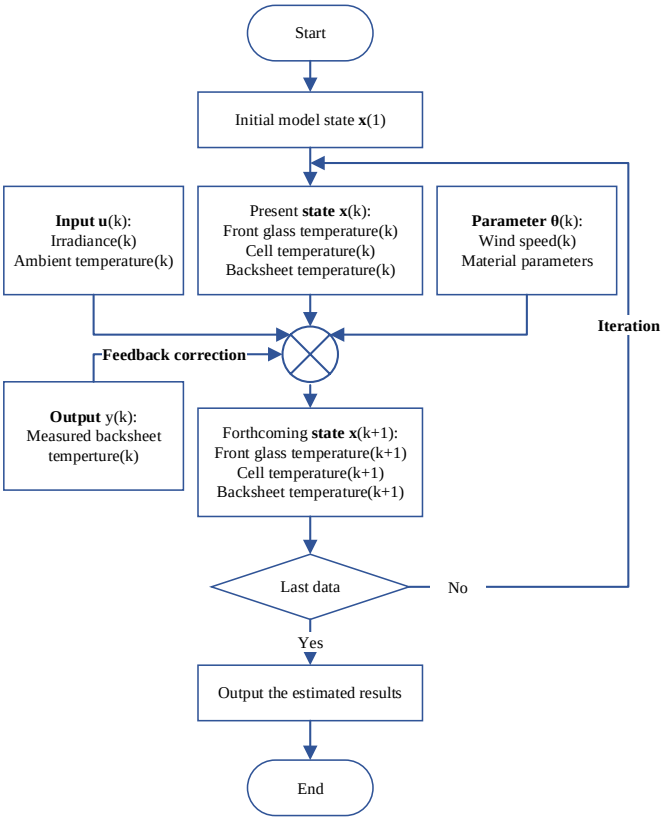

Fig. 2. Flowchart of the MSM-O, in which **x**(1) means the given initial value of temperatures that are chosen to be equal to the ambient temperature and backsheet temperature without loss of generality.

Sandia model [17]:

$$T_c = T_b + \frac{G}{1000}\Delta T \tag{8}$$

where ΔT = 3 ℃ for the module type of the Glass/cell/polymer sheet with open rack mounting.

NOCT model [13]:

$$T_c = T_a + (T_{NOCT} - 20)\frac{G}{800} \tag{9}$$

with T_{NOCT} = 45.7 ℃ according to the datasheet of REC 245 PE.

A general one-state thermal model (OSM) is also established. This model characterizes a global energy balance on the module with one equivalent thermal capacity, which is the sum of capacities of different layers, resulting in the uniform temperature throughout layers. Notably, the heat conduction between layers is not considered in this model. The heat balance equation for the entire module can be written as

$$\begin{aligned} &A_m \cdot \sum_{i=1}^{3}(\rho_i \cdot d_i \cdot C_i)\cdot\frac{dT_m}{dt} \\ &= A_m \cdot\left[\alpha_m \cdot G - \left(2+\alpha_1+\alpha_2\right)\cdot h_{cv,a-m}\cdot(T_m - T_a)\right] - P_e \end{aligned} \tag{10}$$

where the subscribe i (i=1,2,3) represents the properties of the layers, T_m is the equivalent uniform temperature of the PV module, α_m is the absorbance of the module, $h_{cv,a-m}$ is the heat convection coefficient between the module and ambient considering both anterior and posterior sides.

There are also many empirical equations available in the literature. Seventeen different implicit empirical correlations, with eleven new modified implicit ones, have been examined in [14]. It has been found that the proposed MRSSI correlation (11) can be easily used to estimate the module temperature with only the irradiance and ambient temperature, which is given as

$$T_m = T_a - 1.52567 + 0.01981336\cdot G - 0.000003451\cdot G^2 \tag{11}$$

When the wind speed is available, the modified Chenni correlation is another model for comparison. This can be expressed as

$$\begin{aligned} T_m = T_a &- 1.93666 + 0.007882\cdot G - 0.0000134647\cdot G^2 \\ &+ 0.0138\cdot G\cdot\left(1+0.031\cdot T_a\right)\cdot\left(1-0.042\cdot W_s\right) \end{aligned} \tag{12}$$

The following metrics are adopted to evaluate and compare the model performance: Normalized Root Mean Square Error (nRMSE), Normalized Mean Absolute Error (nMAE), Normalized Mean Bias Error (nMBE), Mean Absolute Percentage Error (MAPE), Correlation coefficient (CC), and R-squared Statistics (R^2).

IV. Experimental Set-up

Experimental tests were carried out on a PV outdoor test and monitoring platform at Aalborg University based on the *SOL.Connect® meter mpp* PV panel performance monitoring system. The platform consists of an I-V tracer with an integrated MPP tracker, an in-plane matched reference cell and a PT1000 temperature sensor attached on the center of the module back side. Additionally, a weather monitoring station installed nearby is recording the wind speed and ambient temperature. The electrical and environmental parameters are reported in Table 2.

TABLE 2
Measurements of Electrical and Environmental Parameters

Variable	Sensor	Uncertainty
Current (A)	MPP meter	< 1% STC
Voltage (V)	MPP meter	< 1% STC
Irradiance (W/m^2)	Reference cell	< 4%
Cell temperature (℃)	PT1000 (Class B)	< 0.3 ℃
Backsheet temperature (℃)	PT1000 (Class B)	< 0.3 ℃
Ambient temperature (℃)	PT100 (Class B)	< 0.3 ℃
Wind Speed (m/s)	Hygro-thermometer	< 3%

All the electrical data and rapidly changing environmental data are sampled every 10 seconds, as well as the cell and backsheet temperature. The sample rate of other environmental data, e.g., wind speed and ambient temperature, is one minute per sample. In this case, the original data is preprocessed with interpolation. The data recorded from 5:52 in the morning to 18:51 in the afternoon are used to test the established model. The initial cell temperature is chosen to be equal to the ambient temperature. Actually, the proposed model can also work based on the hybrid estimation model presented in [29], when the irradiance measurements are unavailable. With a Convolutional Neural Network (CNN)-based irradiance forecasting model developed in [30], the result in this paper can be used for further power prediction.

To validate the model performance under various climatic conditions, typical days are considered. The first condition is a clear day as shown in Fig. 3(a). In contrast, an overcast condition is the day shown in Fig. 3(b), in which the irradiance level is below 300 W/m^2 for most time of the day. Irradiance in the third condition, i.e., a cloudy day, is fluctuating frequently, and the fourth one is a mixed day, i.e., a combination of the above, which are described in Fig. 3(c) and (d), respectively.

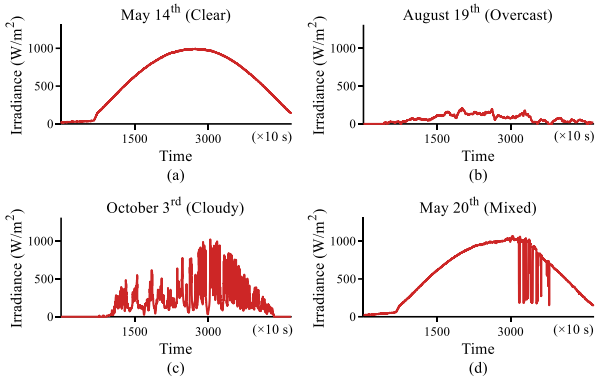

Fig. 3. Solar irradiance levels for different days representing various weather conditions: (a) Clear, (b) Overcast, (c) Cloudy, and (d) Mixed.

Furthermore, data in three months, i.e., May, August, and October in Denmark are specifically chosen. Months in winter are excluded due to the lack of sunlight with an overall irradiance level below 100 W/m^2. In fact, the sunshine duration is quite short in these months, resulting in the maximum power less than 30 W. Boxplots are drawn in Fig. 4 to show the diversities of irradiance in the chosen days. In addition, the wind speed in these chosen months varies dramatically, with a maximum wind velocity of 14.60 m/s, an average of 1.75 m/s, and the standard deviation of 1.60 m/s.

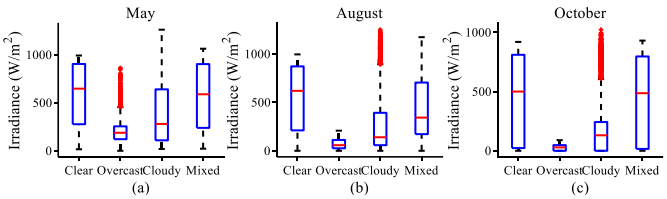

Fig. 4. Boxplots of irradiance under various weather conditions in different months: (a) May, (b) August, and (c) October.

V. Results and Discussion

A. Model validation

Two models, i.e., the MSM and MSM-O, described in the previous sections are established to estimate the temperatures of different layers in the PV module. As an example of the model performance, Fig. 5 shows the estimation results against the measurements for a clear day with detailed residual signals. As it can be seen in Fig. 5, the cell temperature is higher than the backsheet temperature to some extent, especially in the middle of a day. In contrast to the frequently used one-state model, temperatures of different layers can be estimated separately with the proposed model. The results in Fig. 5(b) show that the estimated values coincide well with the measured ones, indicating that the internal behaviors, subject to fluctuating environments, can be well described by the proposed MSM-O. Only small deviations are observed for short periods. In addition, the cell temperature can be tracked more accurately by introducing the measured backsheet temperature, whose role is to adjust the states to correct the estimated errors when using the proposed model. Specifically, most of the estimated residuals of the MSM-O are limited to below 1℃.

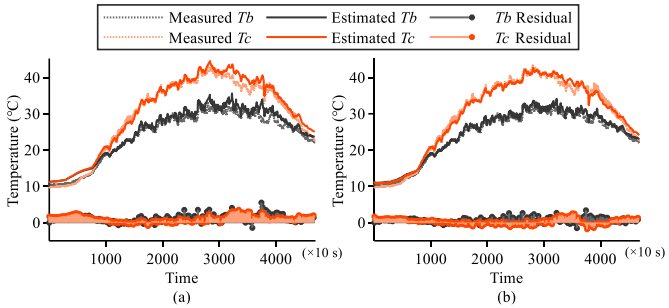

Fig. 5. Temperature estimation results based on the proposed model under a clear day: (a) MSM and (b) MSM-O.

To validate the model performance under different weather conditions, the experiments are conducted on 12 typical days chosen from three months, referring to Figs. 3 and 4. Fig. 6 shows the temperature residual signals under four weather conditions in August.

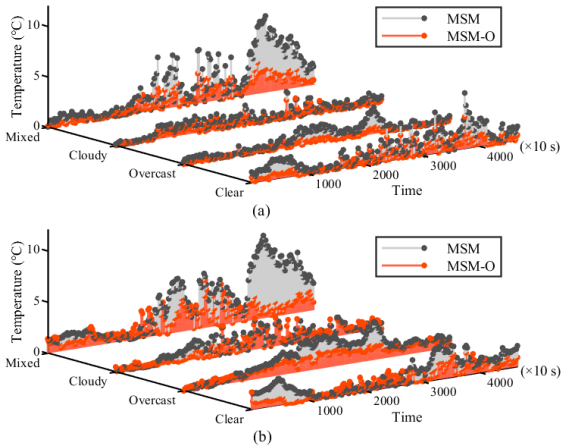

Fig. 6. Estimated temperature residuals under various weather conditions in August: (a) residuals for the backsheet temperature and (b) residuals for the cell temperature.

As observed in Fig. 6, the MSM-O can estimate both the backsheet temperature and cell temperature more accurately under the four weather conditions compared to the MSM. In fact, due to the long-time outdoor exposure, PV modules will encounter various unpredictable problems, which may not be considered in the established model. Using the measured data as feedback can quickly correct the errors. The mean value of the estimated backsheet temperature residual based on the MSM is 0.75 ℃, while it is 0.23 ℃ with the proposed MSM-O. However, the model is less effective for the cell temperature estimation due to more uncertainties with the mean being 1.20 ℃ and 0.49 ℃, respectively.

In addition, Fig. 7 shows the detailed model performance comparison results for four typical days in August. It is noticeable in Fig. 7 that the addition of the backsheet temperature as the feedback can effectively improve the model performance, resulting in the significant reduction in the

indices of nRMSE, nMAE, nMBE and MAPE for various weather conditions. Additionally, larger correlation coefficient and R-squared statistic results show that the estimated temperature is in a close agreement with the measurement, except for the overcast day, August 19th. This can be explained according to Fig. 3(b), where the irradiance is below 200 W/m^2 for the whole day, representing a completely cloudy day. This makes the cell temperature even lower than the backsheet temperature due to the cooling effect. It is inevitable that the dynamic model will fail in this circumstance, as the proposed model is established based on the dynamic process of the heat exchange between the PV module and its surrounding environments. While the similar cell temperature and ambient temperature make the heat exchange no longer the prominent factor. As the output power is below 50 W through the day, the absolute error is negligible.

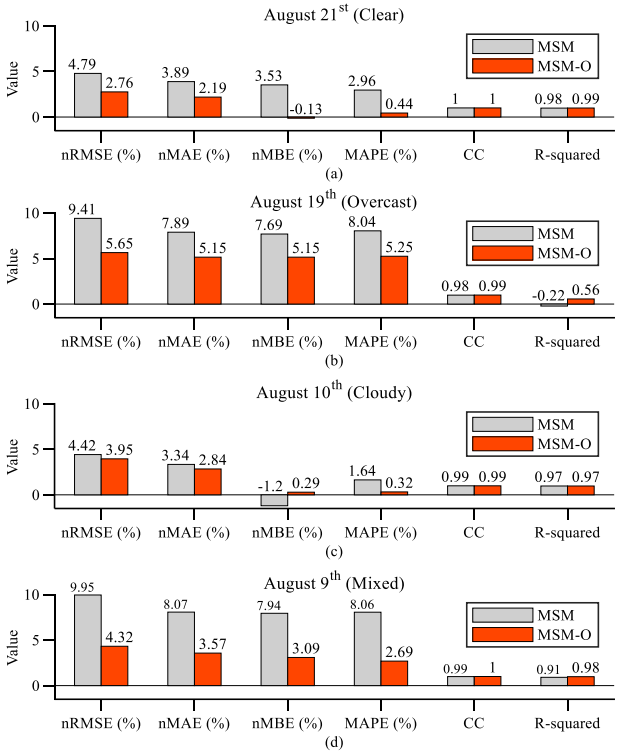

Fig. 7. Model performance comparison for the cell temperature estimation under different weather conditions in August: (a) Clear, (b) Overcast, (c) Cloudy, and (d) Mixed.

To further evaluate the performance of the models, a simple empirical equation is adopted to simulate the output power of the PV module as

$$P_m = P_{STC} \cdot \frac{G}{1000} \cdot \left[1 + \gamma (T_c - 25)\right] \tag{13}$$

where the temperature coefficient γ is −0.4%/°C, and the nominal power under STC P_{STC} is 245 W according to the module datasheet.

The average performance indices for three months under different weather conditions using the MSM and MSM-O, respectively, are listed in Table 3. It can be observed in Table 3 that both models can be used under different weather conditions in the three months, verifying the applicability of the proposed models. By utilizing the observed temperature as the feedback, the nRMSE, nMAE, nMBE and MAPE can be further limited below 5%. High correction coefficient and R-squared statistic results show that the estimation and simulation coincide well with the measured ones, indicating the excellent dynamic model performance under fast-changing environments. As studied in [26], the thermal response time of a solar cell with a silicon thickness of 100–500 μm is around 50–250 s. This means that the internal thermal behavior can be fully described by the proposed model, coordinating with actual environment measurements. Results in Table 3 can further demonstrate that an accurate module temperature estimation is necessary to obtain a reliable simulation of the output power.

TABLE 3
AVERAGE PERFORMANCE INDICES OF THE DEVELOPED MODEL UNDER DIFFERENT WEATHER CONDITIONS

	Backsheet temperature estimation		Cell temperature estimation		Output power simulation	
	n-RMSE	R-squared	n-RMSE	R-squared	n-RMSE	R-squared
Clear						
MSM	0.10	0.91	0.08	0.96	0.03	0.99
MSM-O	0.04	0.98	0.03	0.99	0.02	0.99
Overcast						
MSM	0.04	0.63	0.06	0.46	0.07	0.98
MSM-O	0.02	0.83	0.04	0.77	0.07	0.98
Cloudy						
MSM	0.04	0.95	0.04	0.97	0.03	0.99
MSM-O	0.02	0.98	0.03	0.98	0.03	0.99
Mixed						
MSM	0.17	0.83	0.14	0.90	0.04	0.99
MSM-O	0.05	0.98	0.05	0.98	0.03	0.99

B. Comparison with other models

In this section, the performance of the MSM-O is compared with other representative models. The estimated and measured cell temperature under a clear day, August 21st, are compared in Fig. 8(a). It is observed in Fig. 8(a) that the most precise fit to the measured data is obtained by the proposed MSM-O. The NOCT model overestimates the temperature, while the estimated results of the other models are closer to the backsheet temperature, which is much lower than the actual cell temperature. It is worth noting that the result of the Chenni model, which is closer to the backsheet temperature, is lower than that of the MRSSI. This comparison clearly demonstrates that the introduction of the wind speed can describe the thermal dissipation process better. However, the unique output of these models considers the module as a whole, ignoring the obvious temperature difference between the internal and surface. In addition, the direct relationship between the model output and irradiance in two benchmark models and two empirical correlations makes the estimation results more sensitive to irradiance fluctuations, leading to huge errors. In contrast, the result of the MSM-O is in a good agreement with the experimental results, responding better to transient changes in irradiance.

Based on the estimated temperature, a comparison of the output simulation and actual measurements for the same day is given in Fig. 8(b). A good agreement between the simulation and measurement is achieved based on the MSM-O, indicating the importance of an accurate module temperature estimation to the reliable output power simulation. Due to the negative

correlation between the output power and cell temperature, the NOCT model will underestimate the output, which may cause a false alarm. In contrast, faults will not be detected by the rest of the models, since they overestimate the power.

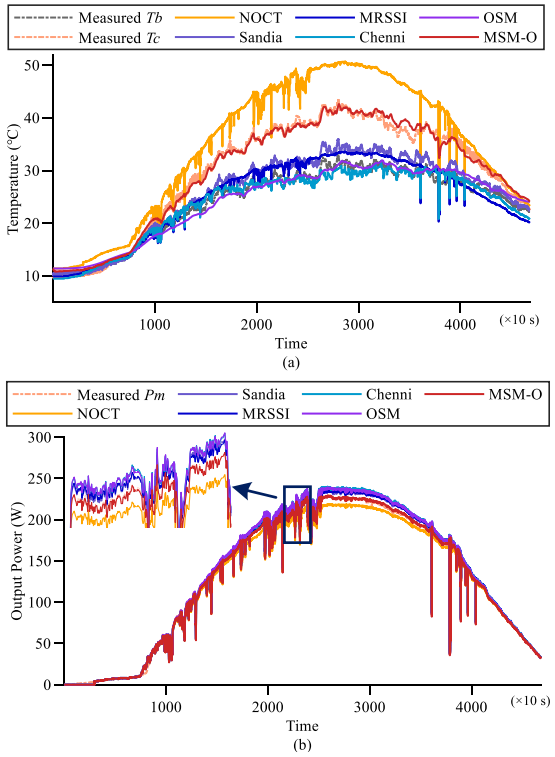

Fig. 8. Comparison of the results based on different models under a clear day: (a) temperature estimation and (b) output power simulation.

To further evaluate the model performance on cell temperature estimation and output power simulation, Figs. 9 and 10 present the corresponding indices under different weather conditions. The proposed MSM-O performs with a comparable accuracy in the estimation and simulation. Markers in different colors gather together for the majority of the performance indices, indicating that the proposed model is robust and applicable for various circumstances. In contrast, other models may just be effective under certain conditions. In particular, the resulting error index RMSE is reduced by more than 50% for the cell temperature estimation and about 30% for the power simulation with respect to the steady-state model based on the NOCT. Although the model does not perform well on overcast days to some extent, compared to the Sandia model, it still outperforms over others. The low irradiance through the day makes the daily output extremely low, meaning that the power simulation error is negligible.

When comparing Figs. 9 and 10, it can be found that the superiority of the MSM-O over other models on the output power simulation is not as remarkable as on the cell temperature estimation. First, the magnitude of the output power is much larger than that of the cell temperature, resulting in a smaller relative error, which makes the gap between models narrow. On the other hand, (13) uses 1000 W/m^2 as the reference irradiance because relevant quantities are easily available from the datasheet given by manufacturers, causing model estimation errors, especially at low irradiation levels. Furthermore, the output power is dependent not only on the irradiance level and cell temperature [31], but also on the degradation degree of the module. All these factors make the simulation based on this empirical equation imprecise. However, the primary objective of this paper is to estimate the cell temperature accurately, rather than to simulate the output power. Simulating the output power based on the estimated temperature is just used to illustrate the significant importance of the operating temperature to the module output. The part of the reliable assessment of the output power will be further developed in the subsequent work.

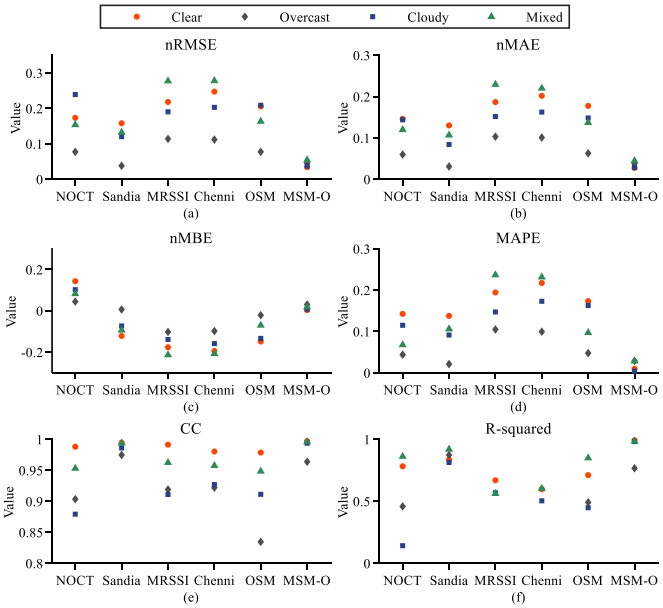

Fig. 9. Model performance comparison for the cell temperature estimation under different weather conditions: (a) nRMSE, (b) nMAE, (c) nMBE, (d) MAPE, (e) CC, and (f) R-squared.

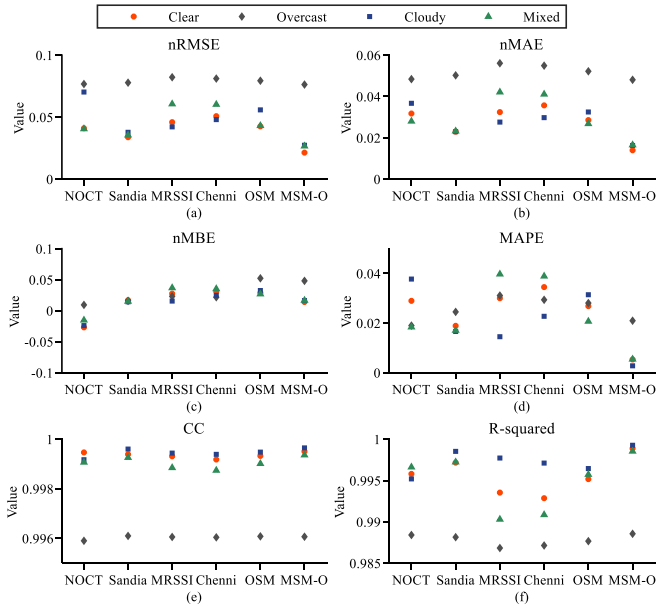

Fig. 10. Model performance comparison for the output power simulation under different weather conditions: (a) nRMSE, (b) nMAE, (c) nMBE, (d) MAPE, (e) CC, and (f) R-squared.

VI. Conclusion

This paper proposed a comprehensive multi-state dynamic thermal model for the PV cell temperature estimation. This

dynamic model considers essential mechanisms of heat transfer between the PV module and its environment, as well as heat conduction between different layers. In addition, different temperatures through the module are modeled as internal states, which are corrected according to the observations. The effectiveness of the proposed model has been demonstrated by experimental validation with outdoor module temperature and performance measurements under different weather conditions. The results have demonstrated the ability of the model to adequately characterize the internal behavior of the modules under normal conditions, when compared with the prior-art steady-state models. The superiority of the proposed model over the one-state thermal model illustrates the necessary of modeling with multiple states to separately estimate the layer temperatures. Furthermore, feedback of actual measurements to compare with the estimated outputs can ensure the timely state correction under certain unforeseen circumstances. In fact, the estimated cell temperature in this paper is a predicted value for the next sampling time, since the estimation is based on the previous estimated results and present measurements. This makes the proposed model further beneficial to predict the output power.

REFERENCES

[1] K. Kant, A. Shukla, A. Sharma, and P. H. Biwole, "Thermal response of poly-crystalline silicon photovoltaic panels: Numerical simulation and experimental study," *Solar Energy*, vol. 134, pp. 147-155, 2016.

[2] S. Regondi, H. Hanifi, and J. Schneider, "Modeling and Simulation of the Influence of Interconnection Losses on Module Temperature in Moderate and Desert Regions," *IEEE Journal of Photovoltaics*, vol. 9, no. 5, pp. 1449-1455, 2019.

[3] G. Farivar and B. Asaei, "A new approach for solar module temperature estimation using the simple diode model," *IEEE transactions on energy conversion*, vol. 26, no. 4, pp. 1118-1126, 2011.

[4] M. M. Rahman, M. Hasanuzzaman, and N. A. Rahim, "Effects of operational conditions on the energy efficiency of photovoltaic modules operating in Malaysia," *Journal of cleaner production*, vol. 143, pp. 912-924, 2017.

[5] E. L. Meyer and E. E. Van Dyk, "Assessing the reliability and degradation of photovoltaic module performance parameters," *IEEE Transactions on reliability*, vol. 53, no. 1, pp. 83-92, 2004.

[6] M. C. C. de Oliveira, A. S. A. D. Cardoso, M. M. Viana, and V. d. F. C. Lins, "The causes and effects of degradation of encapsulant ethylene vinyl acetate copolymer (EVA) in crystalline silicon photovoltaic modules: A review," *Renewable and Sustainable Energy Reviews*, vol. 81, pp. 2299-2317, 2018.

[7] J. Kurnik, M. Jankovec, K. Brecl, and M. Topic, "Outdoor testing of PV module temperature and performance under different mounting and operational conditions," *Solar Energy Materials and Solar Cells*, vol. 95, no. 1, pp. 373-376, 2011.

[8] C. F. Abe, J. B. Dias, P. Poggi, and B. Pillot, "Combining Identification and Translation Methods of the Single-Diode Model to Compute the Average Temperature of Photovoltaic Modules From the Open-Circuit Voltage," *IEEE Journal of Photovoltaics*, vol. 9, no. 5, pp. 1398-1404, 2019.

[9] M. M. Escribano, M. G. Solano, Í de la Parra Laita, J. M. Álvarez, L. Marroyo, and E. L. Pigueiras, "Module Temperature Dispersion Within a Large PV Array: Observations at the Amareleja PV Plant," *IEEE Journal of Photovoltaics*, vol. 8, no. 6, pp. 1725-1731, 2018.

[10] E. Skoplaki and J. A. Palyvos, "Operating temperature of photovoltaic modules: A survey of pertinent correlations," *Renewable energy*, vol. 34, no. 1, pp. 23-29, 2009.

[11] L. S. Pantic, T. M. Pavlović, D. D. Milosavljević, I. S. Radonjic, M. K. Radovic, and G. Sazhko, "The assessment of different models to predict solar module temperature, output power and efficiency for Nis, Serbia," *Energy*, vol. 109, pp. 38-48, 2016.

[12] M. Akhsassi *et al.*, "Experimental investigation and modeling of the thermal behavior of a solar PV module," *Solar Energy Materials and Solar Cells*, vol. 180, pp. 271-279, 2018.

[13] *Photovoltaic devices - Part 5: Determination of the equivalent cell temperature (ECT) of photovoltaic (PV) devices by the open-circuit voltage method*, 2011.

[14] C. Coskun, U. Toygar, O. Sarpdag, and Z. Oktay, "Sensitivity analysis of implicit correlations for photovoltaic module temperature: A review," *Journal of Cleaner Production*, vol. 164, pp. 1474-1485, 2017.

[15] Z. Zhen, X. Taoyun, S. Yanping, L. Wang, P. Jia, and J. Yu, "A method to test operating cell temperature for BIPV modules," *IEEE Journal of Photovoltaics*, vol. 6, no. 1, pp. 272-277, 2015.

[16] V. D. Rumyantsev *et al.*, "Evaluation of the pv cell operation temperature in the process of fast switching to open-circuit mode," *IEEE Journal of Photovoltaics*, vol. 5, no. 6, pp. 1715-1721, 2015.

[17] D. L. King, J. A. Kratochvil, and W. E. Boyson, *Photovoltaic array performance model*. United States. Department of Energy, 2004.

[18] K. Nishioka, K. Miyamura, Y. Ota, M. Akitomi, Y. Chiba, and A. Masuda, "Accurate measurement and estimation of solar cell temperature in photovoltaic module operating in real environmental conditions," *Japanese Journal of Applied Physics*, vol. 57, no. 8S3, p. 08RG08, 2018.

[19] S. Armstrong and W. Hurley, "A thermal model for photovoltaic panels under varying atmospheric conditions," *Applied Thermal Engineering*, vol. 30, no. 11-12, pp. 1488-1495, 2010.

[20] W. Hayes and L. Ngan, "A time-dependent model for CdTe PV module temperature in utility-scale systems," *IEEE Journal of Photovoltaics*, vol. 5, no. 1, pp. 238-242, 2014.

[21] A. Jones and C. Underwood, "A thermal model for photovoltaic systems," *Solar energy*, vol. 70, no. 4, pp. 349-359, 2001.

[22] D. T. Lobera and S. Valkealahti, "Dynamic thermal model of solar PV systems under varying climatic conditions," *Solar energy*, vol. 93, pp. 183-194, 2013.

[23] M. U. Siddiqui, A. F. Arif, L. Kelley, and S. Dubowsky, "Three-dimensional thermal modeling of a photovoltaic module under varying conditions," *Solar energy*, vol. 86, no. 9, pp. 2620-2631, 2012.

[24] L. Migliorini, L. Molinaroli, R. Simonetti, and G. Manzolini, "Development and experimental validation of a comprehensive thermoelectric dynamic model of photovoltaic modules," *Solar Energy*, vol. 144, pp. 489-501, 2017.

[25] M. E. A. Slimani, M. Amirat, I. Kurucz, S. Bahria, A. Hamidat, and W. B. Chaouch, "A detailed thermal-electrical model of three photovoltaic/thermal (PV/T) hybrid air collectors and photovoltaic (PV) module: Comparative study under Algiers climatic conditions," *Energy conversion and management*, vol. 133, pp. 458-476, 2017.

[26] Y. Du *et al.*, "Evaluation of photovoltaic panel temperature in realistic scenarios," *Energy Conversion and Management*, vol. 108, pp. 60-67, 2016.

[27] J. S. Barroso, N. Barth, J. Correia, S. Ahzi, and M. Khaleel, "A computational analysis of coupled thermal and electrical behavior of PV panels," *Solar Energy Materials and Solar Cells*, vol. 148, pp. 73-86, 2016.

[28] M. Rahman, M. Hasanuzzaman, and N. Rahim, "Effects of various parameters on PV-module power and efficiency," *Energy Conversion and Management*, vol. 103, pp. 348-358, 2015.

[29] T. Zhu, L. Xie, H. Wei, H. Wang, X. Zhao, and K. Zhang, "Clear-sky direct normal irradiance estimation based on adjustable inputs and error correction," *Journal of Renewable and Sustainable Energy*, vol. 11, no. 5, p. 056101, 2019.

[30] X. Zhao, H. Wei, H. Wang, T. Zhu, and K. Zhang, "3D-CNN-based feature extraction of ground-based cloud images for direct normal irradiance prediction," *Solar Energy*, vol. 181, pp. 510-518, 2019.

[31] K. J. Sauer, T. Roessler, and C. W. Hansen, "Modeling the irradiance and temperature dependence of photovoltaic modules in PVsyst," *IEEE Journal of Photovoltaics*, vol. 5, no. 1, pp. 152-158, 2014.